frontiers in Materials

ORIGINAL RESEARCH
published: 17 April 2019
doi: 10.3389/fmats.2019.00060

# Regenerated Silk and Carbon Nanotubes Dough as Masterbatch for High Content Filled Nanocomposites

*Luca Valentini*[1]*, *Silvia Bittolo Bon*[1], *Manoj Tripathi*[2], *Alan Dalton*[2] and *Nicola M. Pugno*[3,4,5]*

[1] INSTM Research Unit, Civil and Environmental Engineering Department, University of Perugia, Terni, Italy, [2] Department of Mathematics and Physical Sciences, University of Sussex, Brighton, United Kingdom, [3] Laboratory of Bio-Inspired and Graphene Nanomechanics, Department of Civil, Environmental and Mechanical Engineering, University of Trento, Trento, Italy, [4] School of Engineering and Materials Science, Queen Mary University of London, London, United Kingdom, [5] Ket-Lab, Edoardo Amaldi Foundation, Rome, Italy

Regenerated silk (RS) is a natural polymer that results from the aggregation of liquid silk fibroin proteins. In this work, we observed that RS dispersed in aqueous solution undergoes a reversible solid/liquid transition by programmed heating/cooling cycles. Fourier transform infrared, atomic force microscopy imaging and Raman measurements of the RS reveal that the transition from random coil to β-sheet structures is involved in this liquid–solid transition. The reversible solid-liquid transition of silk fibroin was then found to be helpful to prepare polymer-like carbon nanotube (CNT) dispersions. We demonstrate that the gelation of RS makes the CNTs with the consistency of a dough with polymeric behavior. Such RS can disperse carbon nanotubes at high concentrations of tens of weight percent. Finally, such carbon nanotube dough has been used for the realization of rubber composites. With this method, we pave the way for handling nanopowders (e.g. CNTs or graphene related materials) with safety and reducing the filler volatility that is critical in polymer-processing.

**Keywords: carbon nanotubes, regenerated silk, phase transitions, electrical conductivity, polymer composites**

OPEN ACCESS

***Edited by:***
*Yu Dong,*
*Curtin University, Australia*

***Reviewed by:***
*Francesca Lionetto,*
*University of Salento, Italy*
*Maria Conceição Paiva,*
*University of Minho, Portugal*

***Correspondence:**
*Luca Valentini*
*luca.valentini@unipg.it*
*Nicola M. Pugno*
*nicola.pugno@unitn.it*

***Specialty section:***
*This article was submitted to Polymeric and Composite Materials, a section of the journal Frontiers in Materials*

***Received:*** *12 November 2018*
***Accepted:*** *25 March 2019*
***Published:*** *17 April 2019*

***Citation:***
*Valentini L, Bittolo Bon S, Tripathi M, Dalton A and Pugno NM (2019) Regenerated Silk and Carbon Nanotubes Dough as Masterbatch for High Content Filled Nanocomposites. Front. Mater. 6:60. doi: 10.3389/fmats.2019.00060*

## INTRODUCTION

Regenerated silk (RS) is a natural polymer made by the coagulation of silk fibroin that is a an aggregation of proteins with short and long chains; the combination of intermolecular interactions via hydrogen bonds between the chains leads to the formation of β-sheet structures that have a high crystalline local order. Increasing the fibroin concentration in a solution enhances the probability to generate chain interactions where the β-sheets form a stable gel transition. The dehydration of such crystalline structures results in an irreversible liquid-solid transition due to thermodynamic cross-linking of the β-structures that undergo gelation with time (Ayub et al., 1993; Hanawa et al., 1995; Kang et al., 2000; Wang et al., 2008). Some physical and/or chemical methods have been proposed to enhance the gelation kinetics of silk fibroin, including pH change, mechanical sonication and addition of salts (Matsumoto et al., 2006; Gong et al., 2012; Wu et al., 2012; Kapoor and Kundu, 2016). A reversible sol-gel transition of silk fibroin exposed to acidic or basic vapors and, more recently, in hydrogel-based silk fibroin have also been reported (Terry et al., 2004; Yin et al., 2017).

Liu et al. (2014) demonstrated the thixotropy (i.e., a time dependent shear thinning property) of silk fibroin via dissolution nanofibrils gel in alcohol and sodium chloride while Bai et al. (2014) also showed a reversible sol—gel transition by self-assembly of nanofibers into supramolecular

aggregations without altering the β-sheet contents. Numata et al. (2011) reported the gelation of the regenerated silk induced with ethanol and with a heterogeneous network structure made of a β-sheet and fibrillar structures.

The shape, dimension and the aspect ratios over 1,000 of carbon nanotubes (CNTs) with their ability to undergo large deformations without damage suggests that interesting parallels may be drawn with silk fibroin. However, attention turns to their behavior and potential processability in liquid suspension. There are a lot of experiments done with most common solvents to get stable dispersions of CNTs (Fukushima et al., 2003; Bergin et al., 2009; Davis et al., 2009); however, generally the most common solvents used, such as N-methyl-2-pyrrolidone, dimethylformamide, and 1,2-dichrolobenzene, can disperse only CNTs with specific size and dimension at low concentrations. Recently, Chiou et al. (2018) dispersed carbon nanotube powders in *m*-cresol at very high concentrations giving them a dough-like consistency. However, *m*-cresol is highly volatile, and the processing requires a controlled environment.

In this study we exploit the utilization of salts to dramatically reduce the gelation time of silk fibroin. The results demonstrate that regenerated silk drop solution can undergo liquid-solid transitions within a few min by thermal annealing. The proposed method induced a rapid gelation of CNTs that, when added to RS solution at high concentrations up to tens of weight percent, show a transition dough state that exhibit polymer-like and viscoelastic properties. Finally, as proofs of the concept, such polymer-like CNTs were used as masterbatch to realize a rubber composite.

## MATERIALS AND METHODS

For the preparation of RS film, commercial *B. mori* silk cocoons were boiled for 1 h in distillated water solution of 0.025 wt % $NaHCO_3$, rinsing with distillated water every 30 min to remove the sericin. The degummed silk (i.e., 0.23 g) was then added to a $CaCl_2$ (i.e., 24 g)—water (i.e., 68 ml)—ethanol (i.e., 55 ml) solution and stirred 12 h at 40°C yielding an 1 wt % solution. NANOCYL® NC7000™ multi-walled carbon nanotube powder (average diameter 9.5 nm, average length 1.5 μm, volume resistivity $10^{-4}$ Ohm*cm) was used. In 1 ml of solution, 10 mg of CNTs up to 50 and 2 mg of regenerated silk were dispersed to yield, at maximum, a RS concentration of about 4 wt%. The liquid-solid transition was monitored by the optical density (OD) method, measuring the absorbance at wavelength 550 nm and temperature of 80°C at different times. Fourier transform infrared (FTIR) analysis was performed in a Jasco FTIR FT/IR-615 spectrometer, equipped with an ATR mode in the wave number range from 400 to 4,000 $cm^{-1}$. The spectra were deconvoluted by firstly smoothing the signal with a polynomial function with a 15-point Savitski—Golay smoothing function, subtracting a linear baseline and applying Gaussian deconvoluting curves by Origin 9 software. Rheological data for the RS/CNT dough were recorded on circular specimens (ca. 12 mm wide, and 0.13 mm thick) on an ARES rheometer (Rheometric Scientific). Frequency and strain sweeps, as well as constant strain amplitude, were performed at constant temperature to find the storage modulus (G′) and the loss modulus (G″) of RS and RS/CNT samples at different CNT concentrations. The electrical resistance of the RS/CNT solid dough was obtained with a Keithley 6517B electrometer/high resistance meter equipped with an 8009 test fixture, according to the ASTMD257 that is the worldwide laboratory standard for sensitive measurements. Briefly, the basic method used to determine the resistance is a two-step method: first a test voltage is applied to the sample and the subsequent current is measured; then, the test voltage value and measured current value are applied and the electrical resistance is calculated.

For the atomic force microscopy (AFM) and Raman characterization, dispersion of RS and RS/CNT was drop casted on silicon wafers and glass slides. The sample was heated at 80°C for 1 hour in air conditions. The solid samples were placed in AFM chamber which is an insulated box to minimize environmental noise and building vibration at room temperature. AFM instrument (Model: Bruker Dimension Icon) operated at intermittent contact mode using silicon cantilever (Model: ScanAsist). All the AFM images are produced as a function of time by keeping the other parameters (i.e., scan speed, scan size) constant.

Raman spectroscopy was carried out at room temperature by using 50X objective lens using LASER source of 532nm at 5mW and grating 2400 l/mm. The spectral range was analyzed between 200$cm^{-1}$ to 3000$cm^{-1}$. The Raman spectra were recorded as a function of displacement (i.e. line map) and function of time (i.e. collection of spectra at single region at different time intervals).

For the realization of the polymer composite, an acrylonitrile butadiene rubber (NBR; KNB35), LEVAPREN 700 and vulcanizing agent LUPEROX® F40MF were used. Rubber compounds were prepared by dissolving separately 1.6 g of NBR, 3.1 g of LEVAPREN and 0.25 g of LUPEROX in chloroform and then mixing together with RS/CNTs dough with a DISPERMAT$^{(R)}$ and left to evaporate onto a Teflon mold until the complete evaporation of the solvent was achieved. Carbon nanotubes powder, for a comparison purpose, was sequentially added to the rubber by melt mixing (Banbury mixer) at about 100°C for 10 min. The vulcanizing agent was added just before the extraction of the composite to avoid any cross-linking effect. The composites prepared with both procedures were then vulcanized at 180°C for 5 min in a thermofluid-heated press.

Tensile properties were measured according to ASTM D 412 specifications, on an Instron dynamometer (Model 4301), at 25°C at a crosshead speed of 500 mm $min^{-1}$. At least five specimens of each sample type were tested. The samples were then cut into dumbbell specimens Die A with dimension of ∼140 × 25 × 2 mm.

## RESULTS AND DISCUSSION

The liquid RS extracted from solution and a drop cast on silicon substrate at 80°C shows a liquid–solid transition (**Figure 1a**) that recovers the liquid state under cooling at 25°C within few minutes, which is lower than that of conventional silk-fibroin

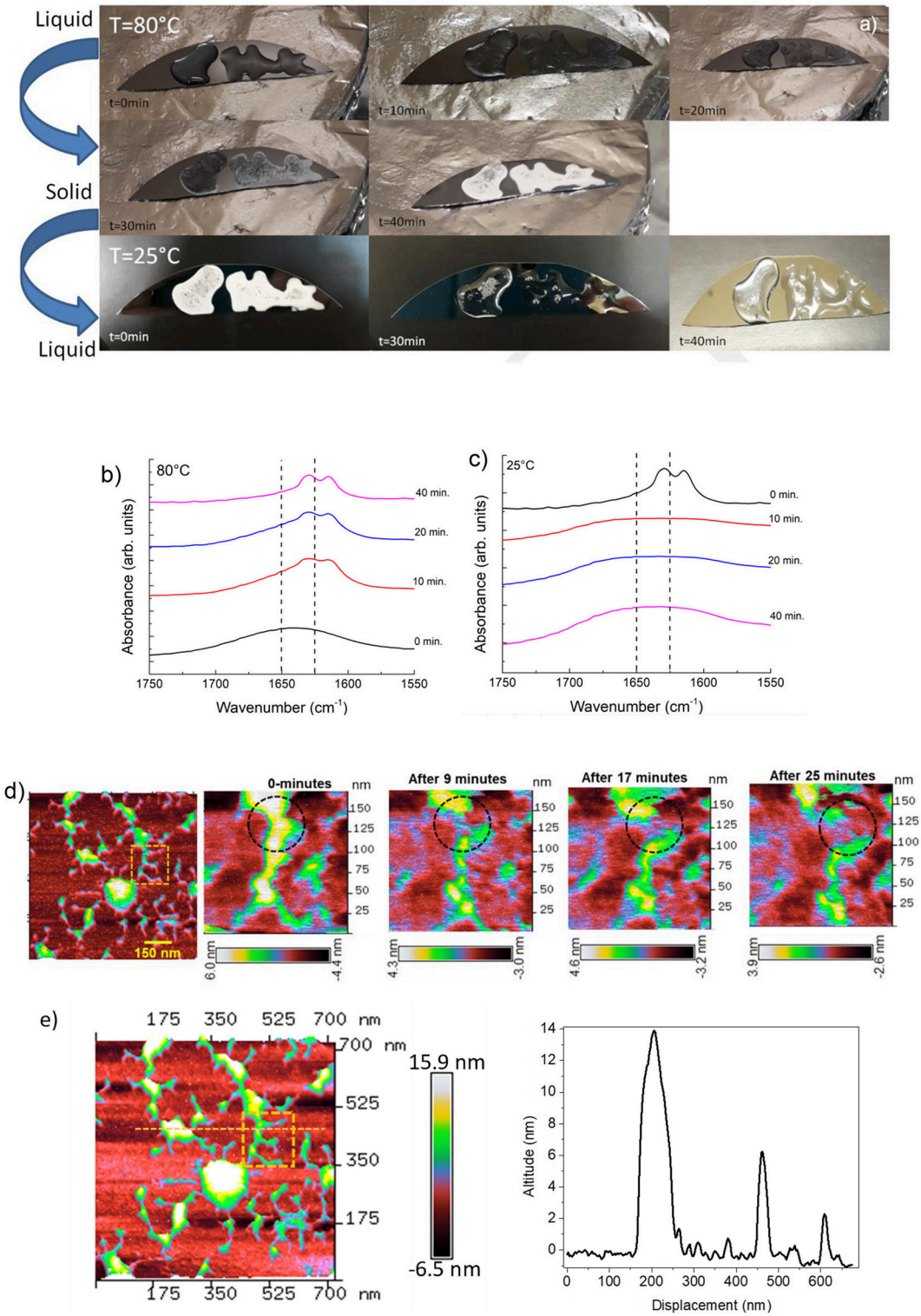


**FIGURE 1 | (a)** Photos showing the reversible liquid-solid transition observed along the heating/cooling time of RS. **(b)** ATR-FTIR spectra in the amide I region for RS liquid solution annealed at 80°C at different times. **(c)** ATR-FTIR spectra in the amide I region for RS solid phase cooled at room temperature at different times. **(d)** AFM topography of solid silk fibroin imaged at different time intervals at room temperature are showing dendritic structure of silk fibroin with several branches. The inset represents a peculiar region analyzed at different time intervals. AFM topography of a zoomed region analyzed up to 25 min; a transformation in the silk-fibroin structure is marked by dashed circle. The scale bar represents the degradation of the structure as a function of time. **(e)** AFM image of the dendritic fibroin network; the dashed line represent the topographic profile of different altitude of the fibroin structure.

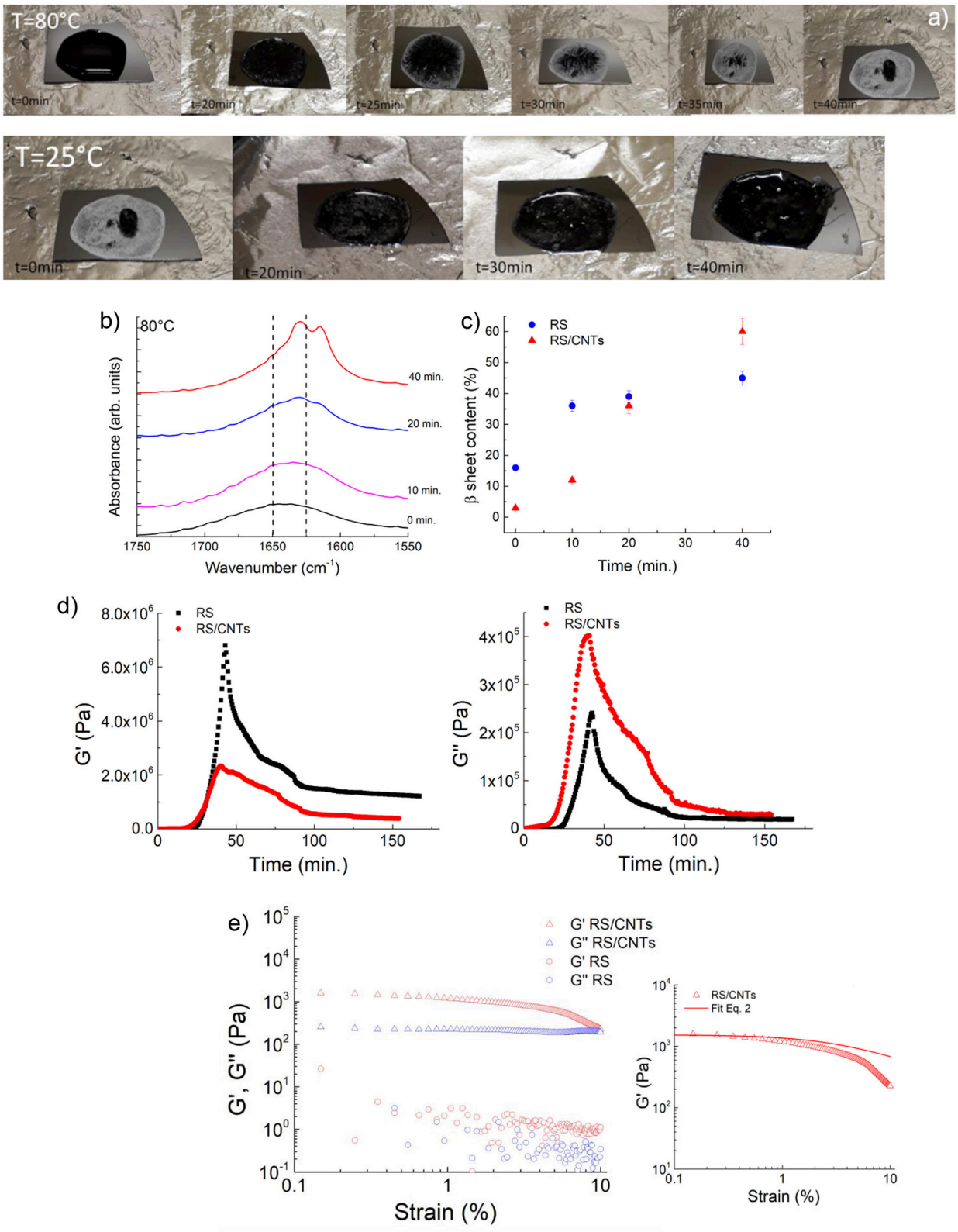


**FIGURE 2 | (a)** Photos showing the reversible liquid-solid transition observed along the heating/cooling time of RS/CNTs. **(b)** ATR-FTIR spectra in the amide I region for RS/CNTs liquid solution annealed at 80°C at different times. **(c)** Annealing time effect on β-sheet content at 80°C assessed by FTIR amide I band analysis for RS

*(Continued)*

**FIGURE 2 |** and RS/CNTs solutions. **(d)** Shear storage (G′) and loss (G″) moduli for RS 2 mg/ml and RS/CNTs dough with a CNT concentration of 50 mg/ml (i.e., 4 wt% RS) measured as a function of time during annealing at 80°C and cooling to 25°C. **(e)** Shear storage (G′) and loss (G″) moduli for RS 2 mg/ml and RS/CNTs dough with a CNT concentration of 50 mg/ml (i.e., 4 wt% RS), measured as a function of shear strain amplitude at 25°C. The plot on the right shows the fit of the storage modulus with Equation 2.

(usually a few weeks) (Matsumoto et al., 2006; Gong et al., 2012). The liquid-solid transition of fibroin results from the formation of physical cross-links made of a β-sheet that makes the optical aspect of the film more opaque. In its liquid state, fibroin is a hydrophobic molecule surrounded by ordered water. In this state, the ordered structure of the water hinders the fibroin aggregation but when the temperature increases, the positive entropic term overwhelms that of heat or enthalpy and local dehydration takes place, enhancing the hydrogen bonding between the chains (Connelly et al., 1964). Increasing the annealing time provides the increased chain interactions through dehydration of the system (Urry et al., 1997), and thus accelerates the solidification.

The RS also exhibits a transition from the solid to the liquid state by setting the substrate at room temperature (**Figure 1a**). Although silk fibroin contains a high content of β-sheet in the solid state, the return to the liquid phase may also imply the existence of metastable fibroin structures within the β-sheet fraction, likely those composed of silk fibroin and $Ca^{2+}$ ions (Ling et al., 2016). Calcium ions can capture water molecules from the atmospheric and hence, the more calcium ion is in silk fibroin solution, the more water molecules, as a solvent, can be captured, resulting in liquid transition.

Changes in the structure of the RS were detected by FTIR analysis. ATR-FTIR spectra of the RS in the amide I region were measured at different times of annealing, as reported in **Figure 1b**. The β-sheet (crystalline) content was determined by the deconvolution of the amide I region and by estimating the ratio between the peak area in the wavenumber region of 1622–1637 $cm^{-1}$, which is the main absorbance region of β-sheet crystal in amide I (Hu et al., 2006), and the whole area of the amide I region comprising the peaks of the structural components, including turns and random coils. The dashed lines mark the adsorption bands at 1650 and 1625 $cm^{-1}$, which are characteristic of the random-coil and β-sheet structures of silk proteins, respectively, according to previous studies (Dong et al., 1990; Goormaghtigh et al., 1990; Mouro et al., 1997; Jung, 2000; Teramoto and Miyazawa, 2005; Tretinnikov and Tamada, 2001). The structure of RS shifted predominantly to a β-sheet structure by increasing the annealing time (**Figure 1b**), whereas random-coil structures are prevalent in the liquid state and vice-versa by cooling at 25°C (**Figure 1c**). The β-sheet content (calculated from the amide I bands over the other main components) in the liquid state was unexpectedly high (≈15%). Moreover, the β-sheet fraction increases with increasing the annealing time and was as high as 45% when the film was completely dry.

**Figure 1d** shows the images of single fibroin molecules obtained by AFM. The concentration of the RS sample was 1 wt %. According to Inoue et al. (2000), the silk fibroin molecule consists of a rodlike part with stringlike parts on each end of the rod. The observed size is 100 nm in width and 14 nm in height (**Figure 1e**). According to the ATR-FTIR analysis, the silk fibroin shows the disappearance of the dendritic structure at different time intervals at room temperature (**Figure 1d**).

The RS/CNT solution, which demonstrated a similar behavior (**Figure 2a**), showed a higher β-sheet content of about 60% once dried (**Figures 2b,c**). More indicative of such transition is the rheological behavior. In **Figure 2d**, the plots of storage (G′) and loss (G″) modulus vs. annealing/cooling cycles (increasing/decreasing values) are shown. According to the interpretation of the FTIR spectra both G′ and G″ increase with annealing time; interestingly both G′ and G″ are independent from the strain for the RS sample, instead they decrease with increasing the strain amplitude for the RS/CNTs sample (**Figure 2e**). For viscoelastic systems filled with rigid solids, this is known as the Payne effect (Payne, 1962). According to this theory, solid fillers may exist in chainlike formation or aggregates within the solid polymer. If there are attractive forces, the particles are held together in single agglomerates that behave like a rigid group under deformation. However, as the magnitude of the stress increases with increasing deformation, these groups will be broken down into smaller units and the elasticity of the material will change. Then, the number of connections N rescales as:

$$N = N_0[1 + (\gamma/\gamma_c)^{2m}]^{-1} \quad (1)$$

where, $N_0$ is the initial connection density, m is the network structure factor, $\gamma$ and $\gamma_c$ are the strain and the yield strain, respectively. This leads to the equation:

$$G' = G'_\infty + (G'_0 - G'_\infty)/[1 + (\gamma/\gamma_c)^{2m}] \quad (2)$$

where $G'_0$ or $G'_\infty$ are the storage moduli at low or high strain, respectively. The best fit of the data (e.g. 0.53) reported in **Figure 2e** with Equation 2 results in a structure factor close to m = 0.5, which is typical for filled elastomers. From the rheological study, we can assume that the RS/CNTs sample behaves as a viscoelastic material.

RS can process CNTs up to tens of weight percent; the photos in **Figures 2a**, **3a** show the liquid CNT solution and its dough state as the annealing time in RS was increased. After drying at 80°C, a disk-shaped sample shrinks isotropically maintaining its shape, resulting in a stiff solid object that could be further handled (**Figure 3a**). Upon cooling, the dough-like state remains stable for at least 20 min (**Figures 2a**, **3a**). As reported in the FESEM images of **Figure 3b**, the CNTs are well-dispersed by the RS. From this analysis, we suggest that the interaction between silk fibroin and CNTs allows their dispersion.

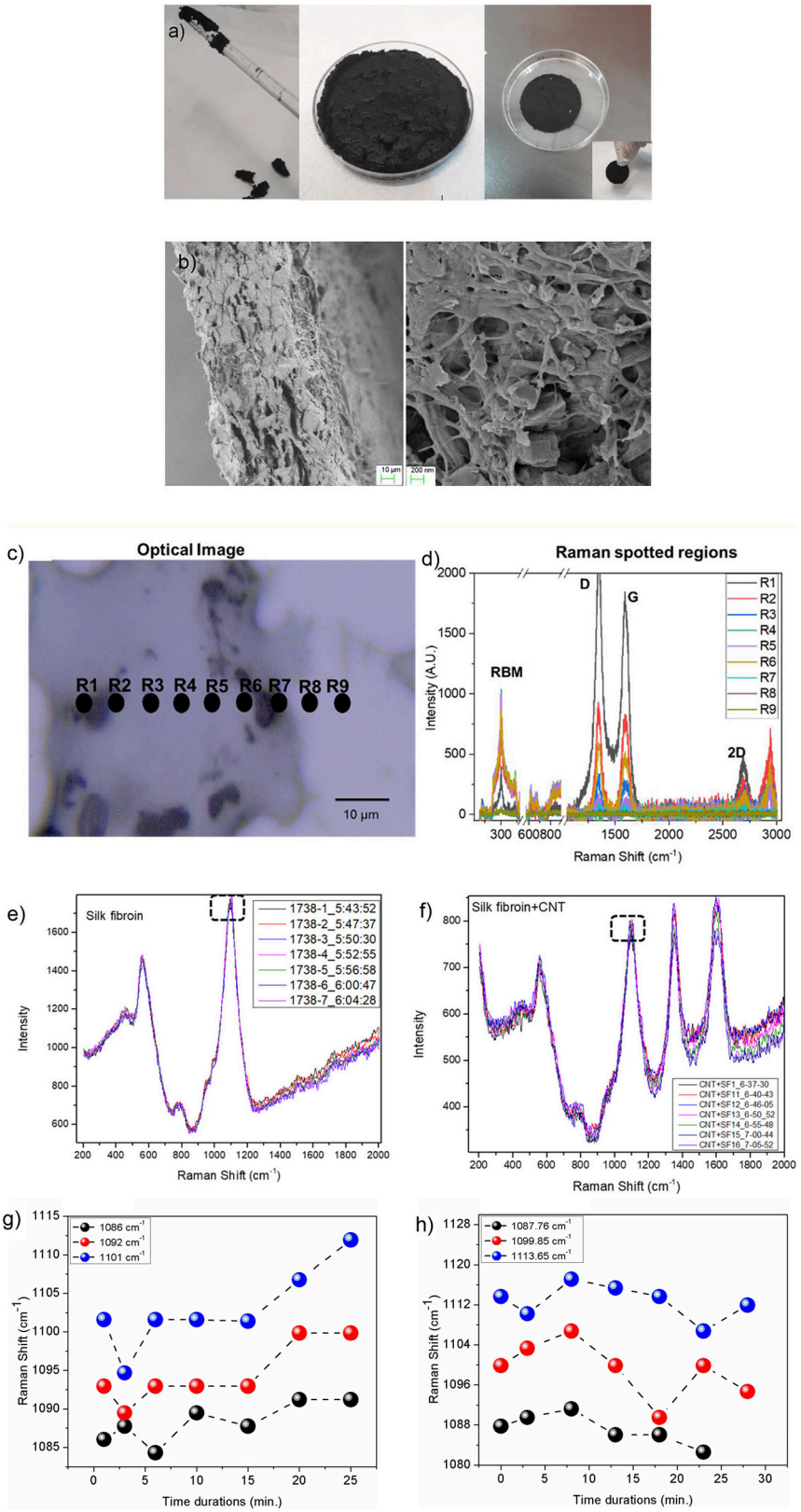


**FIGURE 3 | (a)** The CNTs in RS solution can be processed to obtain a dough. Once annealed, the RS/CNT dough shows a contraction and can be taken by hands as a freestanding solid sample. **(b)** Morphology of RS/CNTs dried sample in FESEM showing well separated CNTs after being processed in RS. **(c)** Optical image of

*(Continued)*

**FIGURE 3 |** RS/CNT showing accumulation of CNT (black regions). Regions marked with R1-R9 are localized spots of Raman spectra. **(d)** Raman spectrum range from 200–3,000 $cm^{-1}$, showing prominent peaks from CNT (RBM, D, G, and 2D), along with peaks from fibroin. Raman spectra of **(e)** RS and **(f)** RS/CNT as a function of time (min) over a glass substrate. Marked dashed rectangle in plots **(e,f)** are analyzed as a function of time. Variation of Raman shift ($cm^{-1}$) for peak positions 1,086, 1,092, and 1,101 $cm^{-1}$ for RS **(g)** and at 1,087, 1099.85, and 1113.65 $cm^{-1}$ for RS/CNT **(h)** monitored up to 24 and 28 min, respectively.

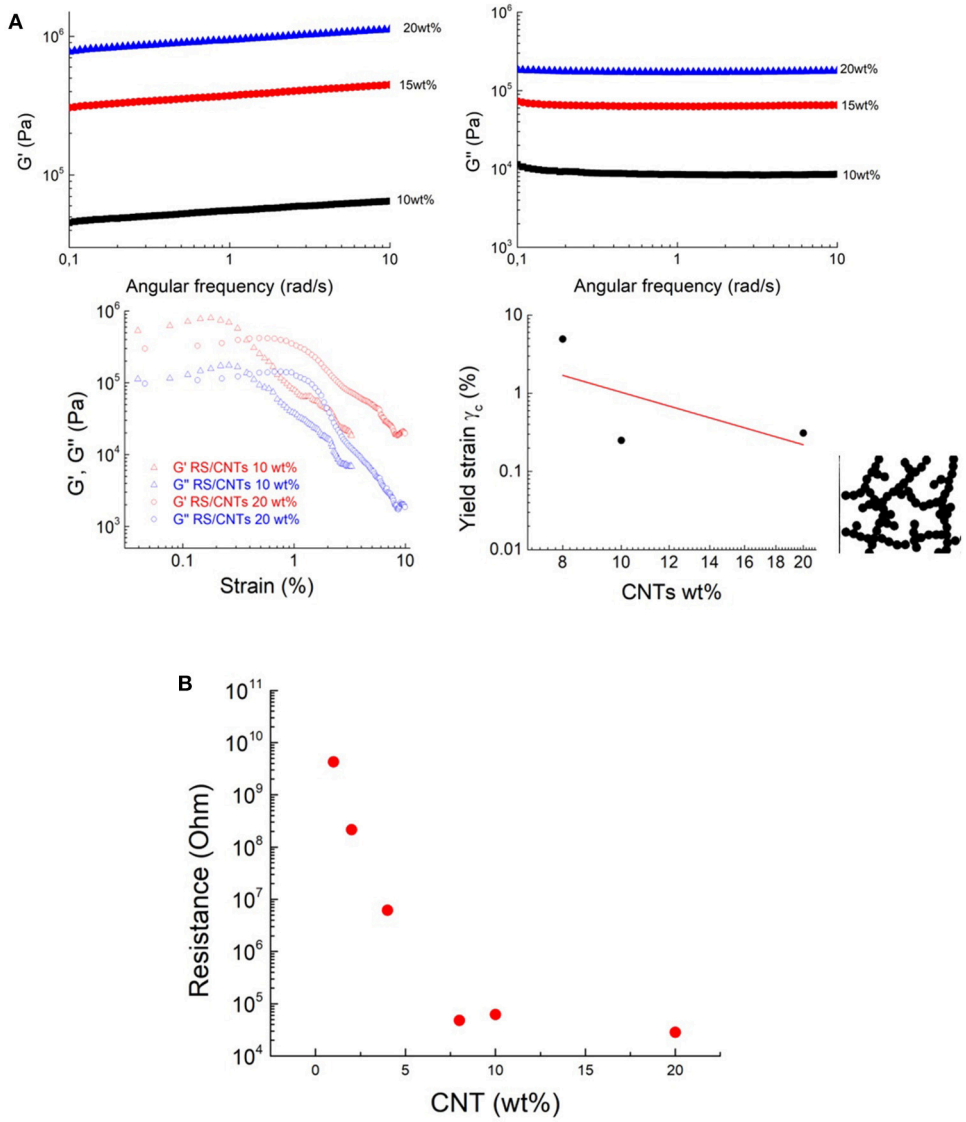


**FIGURE 4 |** The transition to dough-like state is characterized by an increase in a solid-like behavior, based on the results of **(A)** storage moduli (G′) and loss moduli (G") measurements. Shear storage (G′) and loss (G″) moduli RS/CNTs dough with different CNT concentrations, measured as a function of shear strain amplitude at 80°C. Yield strain plotted vs. CNT wt%. The line shows the best fit to Equation 3. Schematic structure of a fractal floc. The flocs are linked to each other. **(B)** Threshold decrease in the electrical resistance of the RS/CNT dough at different CNT concentrations.

In order to confirm this hypothesis, we reported the Raman characterization of RS and RS/CNT samples in **Figures 3c–h**. Raman spectra of the regions reported in **Figure 3c** show the typical Raman features of CNTs i.e., the so-called G-line that is a characteristic feature of the graphitic layers, the defective graphitic structure (D-line), the radial breathing mode (RBM) and the resonant 2D mode (Dresselhaus et al., 2005) (**Figure 3d**). **Figures 3e,g** show the Raman spectra of solid RS, analyzed as a function of time at room temperature. The spectra of **Figure 3e** are similar to those already published (Rousseau et al., 2004) and the assignment of the major bands observed around 600, 800, and 1100 $cm^{-1}$ are based on published Raman results on silk, proteins, and polypeptides (Rousseau et al., 2004). The sub-peaks (**Figures S1–S3** in the Supplementary Material), due to the C-C

stretching vibration at around 1,103 $cm^{-1}$ in the spectrum of the RS, show a blue-shift as a function of time that is associated with the β-sheet reduction, as suggested by Zheng et al. (1989). On the contrary, after addition of CNT in the RS (**Figures 3f,h**), the peak positions at 1,087, 1099.85, and 1113.65 $cm^{-1}$, show a red-shift as a function of time, illustrating a significant contribution from CNT.

The transition to solid state has also been confirmed by rheological, and viscoelastic properties. The transition to polymer-like state suggests that the nanotubes form a cohesive network in RS (Payne, 1962). After annealing, above 10 mg/mL, the CNT network is not free to flow, leading to a freestanding dough (**Figure 3a**). It becomes solid-like with increased storage modulus (**Figure 4A**). The loss modulus decreased more slowly than the storage modulus, giving the dough a sufficient level of viscous character for extrusion. In view of the similarity of our RS/CNTs dough with a viscoelastic medium, as reported in **Figure 2e**, the elastic properties of the samples were modeled by applying the scaling law:

$$\gamma_c \approx f^{-(1+d_B)*(3-d_N)} \quad (3)$$

which have been successfully demonstrated for polymer gels (Shih et al., 1990; Shaffer and Windle, 1992; Boland et al., 2016). These studies showed that both the storage modulus G′ and the limit of linearity of the strain γ (i.e., yield strain $\gamma_c$) exhibit a power-law with respect to particle concentration (f) that is $G' \approx f^{4.1}$ and $\gamma_c \approx f^{-2.1}$ (Sonntag and Russel, 1987; Buscall et al., 1988). Taking the $\gamma_c$ values from **Figures 2e**, **4A** and plotting versus the CNT wt% in **Figure 4A**, we obtain the best fit with a power law with exponent −2.22. Such a value is consistent with the rheological model developed by Shaffer and Windle (1992), who considered the structure of a gel network as a collection of fractal flocs, which are closely packed throughout the sample whit $d_N$ and $d_B$, indicating the fractal dimensions of the network and its backbone, respectively. They observed that in the strong-link regime, where there is an interfloc interaction, the elastic constant (i.e., G′) increases but the limit of linearity (i.e., $\gamma_c$) decreases with increasing particle concentration.

The higher CNT concentrations of this dough-like state are also accompanied by a threshold in the electrical properties. For example, the increase of the CNT concentration from ≈1wt% to ≈10wt% was accompanied by the onset of electrical conductivity (**Figure 4B**), which can be attributed to the start of a percolation threshold, through an interconnected pathway of nanotubes.

The dough state is of potential interest for polymer processing (De Gennes, 1979; Huang et al., 2012; De Volder et al., 2013). The dough can be added to the polymer matrices as masterbatch without handling powders, moreover, the dough state eliminates the use of solvents. **Figure 5** shows the mechanical results of the experiment, where rubber composite has been prepared by blending NBR with RS/CNTs dough. The nanocomposite was then vulcanized under a hot plate press at 180°C. At 10 wt% loading of CNTs in NBR, the toughness modulus of the RS/CNT composite increased by ≈16%, in comparison with a similar composite prepared with CNT powder (**Table 1**). Such preliminary findings suggest that RS/CNTs dough could be used for the processing of polymer nanocomposites.

## CONCLUSIONS

In this study, the transition from solid to liquid state of RS was obtained by the addition of calcium chloride salts to water based silk fibroin solution. It was observed that the presence of salts stimulated the water absorption and this reaction led to a reversible transition. Moreover, the processing parameters including annealing time, allows the control of the molecular organization of silk fibroin in β-sheets structures. Such an inexpensive method to assemble silk in solid state was used for optimizing the dispersion of carbon nanotubes at high concentrations of tens of weight percent. The results show the advantage to use silk fibroin as a natural dispersant to obtain CNTs with the consistency of polymers. As a proof of concept, RS/CNT dough was used to prepare a polymer composite with improved deformability and toughness modulus, with respect to the composite prepared by the addition of CNT powder. Such findings pave the way the utilization of nanopowders dough as master batch in the processing of polymer composites and to overcome the problems of handling nanopowders in industrial implants including graphene and related materials.

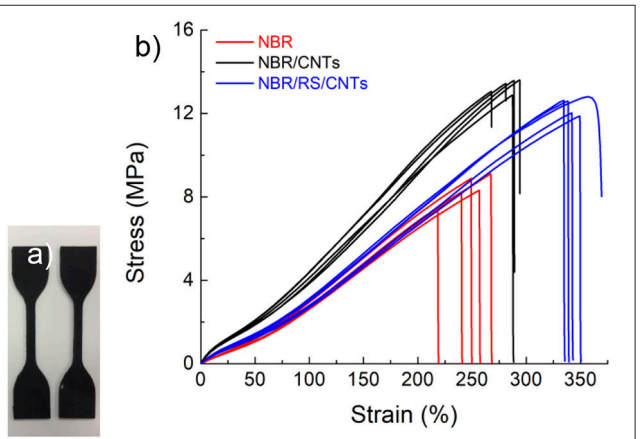


**FIGURE 5 | (a)** Polymer nanocomposite dumbbell specimens obtained by mixing RS/CNTs and NBR. **(b)** Mechanical characterization showing that the polymer composite prepared by mixing NBR with RS/CNT dough at its percolation threshold and CNT powder.

**TABLE 1 |** Polymer nanocomposites (e.g. 10 wt%) mechanical properties (i.e., elongation at break, tensile strength, stress at 50 and 100% of strain and toughness modulus).

| Sample | Elongation at break (%) | Tensile strength (MPa) | Stress at 50% (MPa) | Stress at 100% (MPa) | Toughness modulus (MPa) |
|---|---|---|---|---|---|
| NBR | 246 ± 10 | 8.35 ± 0.39 | 1.5 ± 0.1 | 3.8 ± 0.2 | 10.27 ± 0.24 |
| NBR/CNTs | 283 ± 18 | 13.30 ± 0.44 | 2.0 ± 0.1 | 7.8 ± 0.4 | 18.81 ± 0.31 |
| NBR/RS/CNTs | 344 ± 9 | 12.38 ± 0.49 | 1.5 ± 0.1 | 3.8 ± 0.2 | 21.29 ± 0.30 |

## AUTHOR CONTRIBUTIONS

All authors listed have made a substantial, direct and intellectual contribution to the work, and approved it for publication. In particular SB contributed to the RS and composites realization. MT AFM imaging and its corresponding discussion. AD Raman data and its associated discussion and critical revision.

## FUNDING

NP is supported by the European Commission under the Graphene Flagship Core 2 grant No. 785219 (WP14 Composites) and FET Proactive Neurofibres grant No. 732344 as well as by the Italian Ministry of Education, University and Research (MIUR) under the Departments of Excellence grant L.232/2016. LV is supported by the European Commission under the Graphene Flagship Core 2 grant No. 785219 (WP14 Composites) as well as by the Italian Ministry of Education, University and Research (MIUR) under the Departments of Excellence grant L.232/2016. MT is supported by University of Sussex strategic development fund.

## SUPPLEMENTARY MATERIAL

The Supplementary Material for this article can be found online at: https://www.frontiersin.org/articles/10.3389/fmats.2019.00060/full#supplementary-material

## REFERENCES

Ayub, Z. H., Arai, M., and Hirabayashi, K. (1993). Mechanism of the gelation of fibroin solution. *Biotechnol. Biochem.* 57, 1910–1912. doi: 10.1271/bbb.57.1910

Bai, S., Zhang, X., Lu, Q., Sheng, W., Liu, L., Dong, B., et al. (2014). Reversible hydrogel-solution system of silk with high beta-sheet content. *Biomacromolecules* 15, 3044–3051. doi: 10.1021/bm500662z

Bergin, S. D., Sun, Z., Rickard, D., Streich, P. V., Hamilton, J. P., and Coleman, J. N. (2009). Multicomponent solubility parameters for single-walled carbon nanotube-solvent mixtures. *ACS Nano* 3, 2340–2350. doi: 10.1021/nn900493u

Boland, C. S., Khan, U., Ryan, G., Barwich, S., Charifou, R., Harvey, A., et al. (2016). Sensitive electromechanical sensors using viscoelastic graphene-polymer nanocomposites. *Science* 354, 1257–1260. doi: 10.1126/science.aag2879

Buscall, R., Mills, P. D., Goodwin, J. W., and Lawson, D. (1988). Scaling behaviour of the rheology of aggregate networks formed from colloidal particles. *J. Chem. Soc. Faraday Trans.* 84, 4249–4260. doi: 10.1039/f19888404249

Chiou, K., Byun, S., Kim, J., and Huang, J. (2018). Additive-free carbon nanotube dispersions, pastes, gels, and doughs in cresols. *Proc. Natl. Acad. Sci. U.S.A.* 115, 5703–5708. doi: 10.1073/pnas.1800298115

Connelly, P. R., Aldape, R. A., Bruzzese, F. J., Chambers, S. P., Fitzgibbon, M. J., Fleming, M. A., et al. (1964). Enthalpy of hydrogen bond formation in a protein-ligand binding reaction. *Proc. Natl. Acad. Sci. U.S.A.* 9, 1964–1968.

Davis, V. A., Parra-Vasquez, A.N., Green, M. J., Rai, P. K., Behabtu, N., Prieto, V., et al. (2009). True solutions of single-walled carbon nanotubes for assembly into macroscopic materials. *Nat. Nanotechnol.* 4, 830–834. doi: 10.1038/nnano.2009.302

De Gennes, P. G. (1979). *Scaling Concepts of Polymer Physics.* Ithaca, NY, Cornell University Press.

De Volder, M. F., Tawfick, S. H., Baughman, R. H., and Hart, A. J. (2013). Carbon nanotubes: presentand future commercial applications. *Science.* 339, 535–539. doi: 10.1126/science.1222453

Dong, A., Huang, P., and Caughey, W. S. (1990). Protein secondary structures in water from second-derivative amide I infrared spectra. *Biochemistry.* 29, 3303–3308. doi: 10.1021/bi00465a022

Dresselhaus, M. S., Dresselhaus, G., Saito, R., and Jorio, A. (2005). Raman spectroscopy of carbon nanotubes. *Phys. Rep.* 409, 47–99. doi: 10.1016/j.physrep.2004.10.006

Fukushima, T., Kosaka, A., Ishimura, Y., Yamamoto, T., Takigawa, T., Ishii, N., et al. (2003). Molecular ordering of organic molten salts triggered by single-walled carbon nanotubes. *Science.* 300, 2072–2074. doi: 10.1126/science.1082289

Gong, Z., Yang, Y., Ren, Q., Chen, X., and Shao, Z. (2012). Injectable thixotropic hydrogel comprising regenerated silk fibroin and hydroxypropylcellulose. *Soft Matter.* 8, 2875–2883. doi: 10.1039/c2sm06984a

Goormaghtigh, E., Cabiaux, V., and Ruysschaert, J. M. (1990). Secondary structure and dosage of soluble and membrane proteins by attenuated total reflection Fourier-transform infrared spectroscopy on hydrated films. *J. Biochem.* 193, 409–420.

Hanawa, T., Watanabe, A., Tsuchiya, T., Ikoma, R., Hidaka, M., and Sugihara, M. (1995). New oral dosage form for elderly patients: preparation and characterization of silk fibroin gel. *Chem. Pharm. Bull.* 43, 284–288. doi: 10.1248/cpb.43.284

Hu, X., Kaplan, D., and Cebe, P. (2006). Determining Beta-Sheet Crystallinity in Fibrous Proteins by Thermal Analysis and Infrared Spectroscopy. *Macromolecules* 39, 6161–6170. doi: 10.1021/ma0610109

Huang, J. Q., Zhang, Q., Zhao, and, M. Q., and Wei, F. (2012). A review of the large-scale production of carbon nanotubes: the practice of nanoscale process engineering. *Chin. Sci. Bull.* 57, 157–166. doi: 10.1007/s11434-011-4879-z

Inoue, S.-I., Magoshi, J., Tanaka, T., Magoshi, Y., and Becker, M. (2000). Atomic force microscopy: bombyx mori silk fibroin molecules and their higher order structure. *J. Polymer Sci.* 38, 1436–1439. doi: 10.1002/(SICI)1099-0488(20000601)38:11&<1436::AID-POLB30&>3.0.CO;2-8

Jung, C. (2000). Insight into protein structure and protein–ligand recognition by Fourier transform infrared spectroscopy. *J. Mol. Recognit.* 13, 325–351. doi: 10.1002/1099-1352(200011/12)13:6&<325::AID-JMR507&>3.0.CO;2-C

Kang, G. D., Nahm, J. H., Park, J. S., Moon, J. Y., Cho, C. S., and Yeo, J. H. (2000). Effects of poloxamer on the gelation of silk fibroin. *Marcromol. Rapid Commun.* 21, 788–791. doi: 10.1002/1521-3927(20000701)21:11&<788::AID-MARC788&>3.0.CO;2-X

Kapoor, S., and Kundu, S. C. (2016). Silk protein-based hydrogels: promising advanced materials for biomedical applications. *Acta Biomater.* 31, 17–32. doi: 10.1016/j.actbio.2015.11.034

Ling, S., Zhang, Q., Kaplan, D. L., Omenetto, F., Buehler, M. J., and Qin, Z. (2016). Printing of stretchable silk membranes for strain measurements. *Lab Chip* 16, 2459–2466. doi: 10.1039/C6LC00519E

Liu, Y., Ling, S., Wang, S., Chen, X., and Shao, Z. (2014). Thixotropic silk nano fibril-based hydrogel with extracellular matrix-like structure. *Biomater. Sci.* 2, 1338–1342. doi: 10.1039/C4BM00214H

Matsumoto, A., Chen, J., Collette, A. L., Kim, U. J., Altman, G. H., and Cebe, P., et al. (2006). Mechanisms of silk fibroin sol-gel transitions. *J. Phys. Chem. B* 110, 21630–21638. doi: 10.1021/jp056350v

Mouro, C., Jung, C., Bondon, A., and Simonneaux, G. (1997). Comparative fourier transform infrared studies of the secondary structure and the co heme ligand environment in cytochrome p-450cam and cytochrome p-420cam. *Biochemistry* 36, 8125–8134. doi: 10.1021/bi9700173

Numata, K., Katashima, T., and Sakai, T. (2011). State of water, molecular structure, and cytotoxicity of silk hydrogels. *Biomacromolecules* 12, 2137–2144. doi: 10.1021/bm200221u

Payne, A. R. (1962). The dynamic properties of carbon black-loaded natural rubber vulcanizates. *Part I. J. Appl. Polym. Sci.* 6, 57–63. doi: 10.1002/app.1962.070061906

Rousseau, M. E., Lefèvre, T., Beaulieu, L., Asakura, T., and Pézolet, M. (2004). Study of protein conformation and orientation in silkworm and spider silk fibers using raman microspectroscopy. *Biomacromolecules* 5, 2247–2257. doi: 10.1021/bm049717v

Shaffer, M. S. P., and Windle, A. H. (1992). Analogies between polymer solutions and carbonnanotube dispersions. *Macromolecules* 32, 6864–6866. doi: 10.1021/ma990095t

Shih, W. H., Shih, W. Y., Kim, S. I. Liu, J., and Aksay, I. A. (1990). Scaling behavior of the elastic properties of colloidal gels. *Phys. Rev. A* 42, 4772–4779. doi: 10.1103/PhysRevA.42.4772

Sonntag, R. C., and Russel, W. B. (1987). Elastic properties of flocculated networks. *J. Colloid Interface Sci.* 116, 485–489. doi: 10.1016/0021-9797(87)90144-5

Teramoto, H., and Miyazawa, M. (2005). Molecular orientation behavior of silk sericin film as revealed by atr infrared spectroscopy. *Biomacromolecules* 6, 2049–2057. doi: 10.1021/bm0500547

Terry, A. E., Knight, D. P., Porter, D., and Vollrath , F. (2004). pH Induced changes in the rheology of silk fibroin solution from the middle division of bombyx mori silkworm. *Biomacromolecules* 5, 768–772. doi: 10.1021/bm034381v

Tretinnikov, O. N., and Tamada, Y. (2001). Influence of casting temperature on the near-surface structure and wettability of cast silk fibroin films. *Langmuir* 17, 7406–7413. doi: 10.1021/la010791y

Urry, D. W., Peng, S. Q., Xu, J., and McPherson, D. T. (1997). Modulation of reactivity in native chemical ligation through the use of thiol additives. *J. Am. Chem. Soc.* 19, 11161–11162.

Wang, X., Kluge, J. A., Leisk, G. G., and Kaplan, D. L. (2008). Sonication-induced gelation of silk fibroin for cellencapsulation. *Biomaterials* 29, 1054–1064. doi: 10.1016/j.biomaterials.2007.11.003

Wu, X., Hou, J., Li, M., Wang, J., Kaplan, D. L., and Lu, S. (2012). Sodium dodecyl sulfate-induced rapid gelation of silk fibroin. *Acta Biomater.* 8, 2185–2192. doi: 10.1016/j.actbio.2012.03.007

Yin, Z., Wu, F., Xing, T., Yadavalli, V. K., Kundu, S. C., and Lu, S. (2017). A silk fibroin hydrogel with reversible sol–gel transition. *RSC Adv.* 7, 24085–24096. doi: 10.1039/C7RA02682J

Zheng, S., Li, G., Yao, W., and Yu, T. (1989). Raman spectroscopic investigation of the denaturation process of silk fibroin. *Appl. Spectrosc.* 43, 1269–1272. doi: 10.1366/0003702894203525

**Conflict of Interest Statement:** The authors declare that the research was conducted in the absence of any commercial or financial relationships that could be construed as a potential conflict of interest.

*Copyright © 2019 Valentini, Bittolo Bon, Tripathi, Dalton and Pugno. This is an open-access article distributed under the terms of the Creative Commons Attribution License (CC BY). The use, distribution or reproduction in other forums is permitted, provided the original author(s) and the copyright owner(s) are credited and that the original publication in this journal is cited, in accordance with accepted academic practice. No use, distribution or reproduction is permitted which does not comply with these terms.*